Appl Nanosci (2014) 4:829–838
DOI 10.1007/s13204-013-0262-5

ORIGINAL ARTICLE

Fabrication of nanocubic ZnO/SnO_2 film-based humidity sensor with high sensitivity by ultrasonic-assisted solution growth method at different Zn:Sn precursor ratios

N. D. Md Sin · M. H. Mamat · M. F. Malek · M. Rusop

Received: 15 June 2013 / Accepted: 5 August 2013 / Published online: 1 September 2013

Abstract We fabricated humidity sensor using nanocubic ZnO/SnO_2 prepared via sol–gel and immersion method deposited on sputtered ZnO-film-coated glass substrate. These combination methods were used to grow nanocubic structured ZnO/SnO_2 at different molar ratios Zn:Sn for the first time. The experiment was conducted at difference molar ratio of Zn:Sn by varying the molar of Zn. The size of the cube reduces as the Zn molar increase. The luminescence of nanocubic structured ZnO/SnO_2 was indicated around 400 and 600 nm corresponding to the ultra-violet (UV) emission and visible emission, respectively. The composition of molar ratio 10:10 of nanocubic structured ZnO/SnO_2 gives the best sensitivity of 104 times for humidity sensor properties. Nanocubic structured ZnO/SnO_2 have a great potential for humidity sensor application with high response (411 s) and recovery times (98 s), repeatability and good in stability.

Keyword High sensitivity · Molar ratio Zn:Sn · Nanocubic ZnO/SnO2 · Humidity sensor

Introduction

Humidity sensor is very important for semiconducting industry. This is to avoid any short circuit and damage inside an instrument to control the humidity. The obstacle of a sensor including contamination problems, short lifetime, hysteresis and restricted to certain temperature and humidity always has been an issue (Rittersma 2002). The performance of the humidity sensor can be improved by many factors such as the size of the morphology and the modification of material by doping with other element or metal. The size morphology can be controlled from the process preparation and the molarities of material. The oxide composite material such as $ZnO–TiO_2$ (Gu et al. 2011), $SnO_2–ZnO$ (Hemmati et al. 2011), $SnWO_4–SnO_2$ (Sundaram 2007) and $SnO_2–TiO_2$ (Yadav et al. 2012) have been synthesized to fabricate humidity sensor. In addition, doped metal oxide films such as Pd-doped ZnO (Wang et al. 2007a), Al-doped ZnO (Sin et al. 2011), and KCl-doped SnO_2 (Song et al. 2009) have also been used for humidity sensor fabrications. ZnO/SnO_2 is a well known material that has been extensively investigated for its capability in performing excellently in nanotechnology devices.

The hydrothermal process is simple wet chemical processes that used low processing temperature and provided large-scale production. Various types of ZnO/SnO_2 nanostructure have been reported, such as sphere (Fan et al. 2011), hexagon (Ji et al. 2010), cubic (Lu et al. 2012a) and rods (Jin et al. 2012). These factors are favorable in enhancing sensing performance. Wang et al. (2010) reported on the synthesis of ZnO/SnO_2 cubic structures for formaldehyde (HCHO) sensor by controlling the reaction time, temperature, perform high sensitivity, fast response and recovery times to detect HCHO gas. Hoel et al. (2010) reported the preparation of zinc stannate microcubic growth on ZnO nanorod for liquefied petroleum gas (LPG) sensing and found that the surface modification of ZnO nanorods using zinc stannate microcubes thus increase the sensing performance. Bauskar et al. (2012) synthesized $ZnSnO_3$ microcubes via spin-coating process deposited on alumina substrate exhibit excellent humidity sensing properties.

N. D. Md Sin (✉) · M. H. Mamat · M. F. Malek · M. Rusop
NANO-ElecTronic Centre (NET), Faculty of Electrical Engineering, Universiti Teknologi MARA (UiTM), 40450 Shah Alam, Selangor, Malaysia
e-mail: nordiyana86@yahoo.com

The composition, morphology and performance are correlated to provide high-performance sensor (Ji et al. 2010). Different morphology structure of ZnO–SnO_2 has been developed, such as wire (Fouad et al. 2008), rod (Sun et al. 2011), cones (Sun et al. 2012) and flower-like structure (Li et al. 2006) using various methods including co-precipitations (Lin and Chiang 2012), thermal evaporation (Acharya et al. 2012), hydrothermal (Wang et al. 2007b) and sol–gel method (Martínez et al. 2012). These coupled oxide semiconductor material have their own special properties of their conductance variability and selectivity to different gases. Han et al. (2010) study the doping effect of Fe, Ti and Sn on the gas sensing property of ZnO and the sensing response of Sn–ZnO show the highest. Lu et al. (2012a, b) fabricate gas sensor-based ZnO/SnO_2 composite by controlling the molar ratio Zn:Sn. However, there is less report in synthesizing the composition of molar ratio Zn:Sn for humidity sensor application. In this paper, we emphasize the effect of molar ratio composition of ZnO/SnO_2 that growth on ZnO catalyst by ultrasonic sol–gel and immersion method with low temperature for humidity sensor applications. To the best of our knowledge, nanocubic structured ZnO/SnO_2 with different compositions of molar ratio (Zn:Sn) using ultrasonic sol–gel and immersion method for humidity sensor application has not been reported.

Experimental procedure

ZnO catalyst preparation

ZnO thin films were deposited [high purity (99.999 %)] on glass substrate using radio frequency (RF) magnetron system at RF power 200 W. The pressure of the system was maintained at 7 mTorr and the sputter chamber was pumped at 5×10^{-4} Pa using a molecular pump. The gases were injected into the chamber with ratio of flow rate argon to oxygen (45:5) sccm. The ZnO thin films were deposited for 1 h with substrate temperature 500 °C.

Material preparation

The growths of cubic structured were carried out through the ultrasonic sol–gel immersion. The solutions were prepared using 0.02 M tin(IV) chloride pentahydrate ($SnCl_4 \cdot 5H_2O$) and zinc chloride 6 mM ($ZnCl_2$) with a controlled molar ratio of Zn:Sn of 1:10, 3:10, 5:10, 7:10 and 10:10. Sodium hydroxide (0.2 mol) NaOH used as mineralizer. Each material was dissolved in deionized (DI) water for several minutes and forming clear solution. $SnCl_4$ solution slowly dropped into NaOH solution while stirring using magnetic stirrer until a clear solution was produced. Then $ZnCl_2$ solution was introduced slowly into the NaOH solution under magnetic stirring with the same condition as before. Next, the solution was sonicated at 50 °C to obtain whitish solution. Then, this solution was poured into a Schott bottle, which sputtered ZnO thin films-coated glass substrate placed at the bottom. After that, the bottle was immersed into the water bath at 95 °C for 30 min. The resulting sample was washed with DI water. Finally, the samples were dried at 100 °C for 15 min and annealed at 500 °C for 1 h.

Characterization

The structural properties of the samples were characterized using field emission scanning electron microscopy (FE-SEM, JEOL JSM 6701F), X-ray diffraction (XRD, Rigaku Ultima IV) and energy-dispersive X-ray spectroscopy (EDS). The optical properties were analyzed using photoluminescence (PL) system (Horiba Jobin-Yvon-DU420A-OE-325 system).

Sensor fabrication

The gold (Au) contacts were deposited using sputter coater (EMITECH K550X) for 4 min to achieve 60 nm thickness at deposition current of 50 mA. The distance between the contacts is 66 μm. The characteristics of the sensor were tested using 2 probe I–V measurement (Keithley 2400) controlled by transport measurement system software. The temperature was set at room temperature (25 °C) while relative humidity (RH%) were varied in the range 40–90 RH%.

Results and discussion

Structural properties

Figure 1 shows the FESEM images of highly porous films consisting of nanocubic structured ZnO/SnO_2 that prepared at different molar ratio of Zn:Sn precursors in the ranges between 1:10 and 10:10. The images reveal that all samples were uniformly deposited with monodispersed nanocubic structured ZnO/SnO_2, suggesting the quality nanocubic structured ZnO/SnO_2 film achieved with this approach. The FESEM images also reveal that size of nanocubic structured ZnO/SnO_2 decrease with the increase of molar ratio of Zn precursor over that of Sn precursor. The sizes of nanocubic are in the ranges of 170–220, 100–130, 90–120, 50–90 and 50–70 nm at Zn:Sn precursor molar ratios of 1:10, 3:10, 5:10, 7:10 and 10:10, respectively. On the basis of experimental data obtained above, it can be shown that higher Zn precursor concentration is contributive to the

growth of smaller size of nanocubic structured ZnO/SnO_2. Figure 2a, b show FESEM image of cross-sectional view of molar ratio 1:10 and 10:10 of nanocubic structured ZnO/SnO_2, respectively. The image of cross-sectional view of molar ratio 1:10 indicate agglomerate particles on the ZnO-film-coated glass. However, well-shaped nanocubic structured ZnO/SnO_2 on the ZnO-film-coated glass were clearly shown from the image of cross-sectional view of molar ratio 10:10 as shown in Fig. 2b. From the images of cross section, it can be seen the porosity as indicated with circle of molar ratio 1:10 and 10:10 nanocubic structured ZnO/SnO_2. The thicknesses of all samples were almost the same with average 2.3 μm. The ZnO-film-coated glass has average thickness of 180 nm. The EDS spectrum as shown in Fig. 3 of nanocubic structured ZnO/SnO_2 prepared at molar ratio 10:10 shows the presence of Zn, Sn, and O elements in thin film. The silicon and carbon were also detected that influenced glass peak. The atomic ratio of Zn:Sn:O was 18.46:14.96:60.51. The formation of the nanocubic structured ZnO/SnO_2 can be shown by the following reactions:

$$Sn^{4+} + 6OH^- \leftrightarrow Sn(OH)_6^{2-} \quad (1)$$

$$Zn^{2+} + Sn(OH)_6^{2-} \leftrightarrow Zn(Sn(OH)_6 \quad (2)$$

The form of nanocubic structured ZnO/SnO_2 via hydrothermal are crucially dependent on the characteristics, such as solvent composition, temperature, reaction time, pH and ultrasonic treatment (Tang et al. 2006). The possible formation process of nanocubic structured ZnO/SnO_2 on the ZnO-film-coated glass was simplified into five stages as shown in Fig. 4. First, precursor (Zn and Sn) is dissolved in DI water to form a transparent solution providing Zn^{2+} and Sn^{4+}. Concentrated NaOH was added to Sn^{2+} which reacts with OH^- from the NaOH and produce $Sn(OH)_6^{2-}$ (1), followed by addition of Zn^{2+} into (1) to produce $Zn(Sn(OH)_6$ (2).

Second stage is the combination of (1) and Zn^{2+} solution to form sol–gel solution ($Zn(Sn(OH)_6$) driven by ultrasonic treatment at 50 °C for 5 min to improve ion diffusion rate (Tang et al. 2006). At this stage, the solution was managed during ultrasonic treatment time and temperature to avoid the particles size increases. Third stage was the immersion process inside the water bath at 90 °C for 30 min. At this stage, $Zn(Sn(OH)_6$) solution adheres on the ZnO-film-coated glass. Fourth stage is the attraction of heterogeneous nucleation process between sonication sol–gel solution $Zn(Sn(OH)_6$ on the ZnO-film-coated glass. The reaction temperature permitted the evolution of the particle size to increase and transform into cubic structure due to Ostwald ripening law (Zeng et al. 2007; Cao et al. 2011). Ostwald ripening law explained the occurence of aggregation of particles due to surface tension and surface-to-volume ratio (Fan et al. 2010). Fifth stage is the particle size of $Zn(Sn(OH)_6$ grew up on the ZnO-film-coated glass and formed cubic structured. The heterogeneous nucleation of $Zn(Sn(OH)_6$ nucleate continuously onto ZnO-film-coated glass surface followed by a "dissolution–precipitation" growth process (Wrobel et al. 2009).

The nanocubic structured ZnO/SnO_2 was characterized using XRD. Figure 5 shows the XRD patterns of molar ratio 1:10 and 10:10 of nanocubic structured ZnO/SnO_2, which are indexed as ZnO/SnO2 JCPDS card no. 11-0274. Both samples show dominant XRD peak at (002) orientation that belongs to the ZnO while SnO_2 show weak peaks that implying by other peaks as shown in Fig. 5. The obvious peaks at (002) orientation are influenced by ZnO-coated glass prepared by RF magnetron sputtering. As the addition of molar Zn increased, the peak intensity of (002) of molar ratio 10:10 of ZnO/SnO2 nanocubic increased and the SnO_2 peak intensity more slowly.

Optical properties

Figure 6 shows PL spectra of molar ratio 10:10 nanocubic structured ZnO/SnO_2 excited by He–Cd laser operating at 325 nm. There were two emission bands in the thin film at ultra-violet (UV) emission with low intensity at 408 nm and the broad visible region dominating the peak emission around 600 nm. Some broad peaks at visible region were assigned as around D_1 and D_2 corresponding to existence of the Zn and Sn interstitial defect (Yan et al. 2010). The UV emission contributes to the exciton recombination of electrons in the singly occupied oxygen vacancies (V_o) with photoexcited holes in the valence band inducing the green emission band in the PL spectrum of the sample (Baruah and Dutta 2011; Su et al. 2007; Hadia et al. 2009). The visible peaks were attributed to defects, such as oxygen vacancies in ZnO and SnO_2 and or residual strain temperature during the growth of Zn interstitials. The oxygen vacancies which act as luminescent centers can form defect levels located highly in the gap, trapping electrons from valence band contributing to the luminescence. Most oxygen vacancies will be in their V_o^+ state under flat band conditions as V_o^0 being a superficial donor (Hadia et al. 2009).

Humidity sensor properties

All sensors of nanocubic structured ZnO/SnO_2 were tested at 40 to 90 RH% at constant temperature 25 °C to investigate sensitivity performance towards humidity environment. The fabricated sensors were given supplied bias 5 V. Au metal contact was deposited to act as electrode. Figure 7 shows the *I–V* measurement of molar ratio 10:10

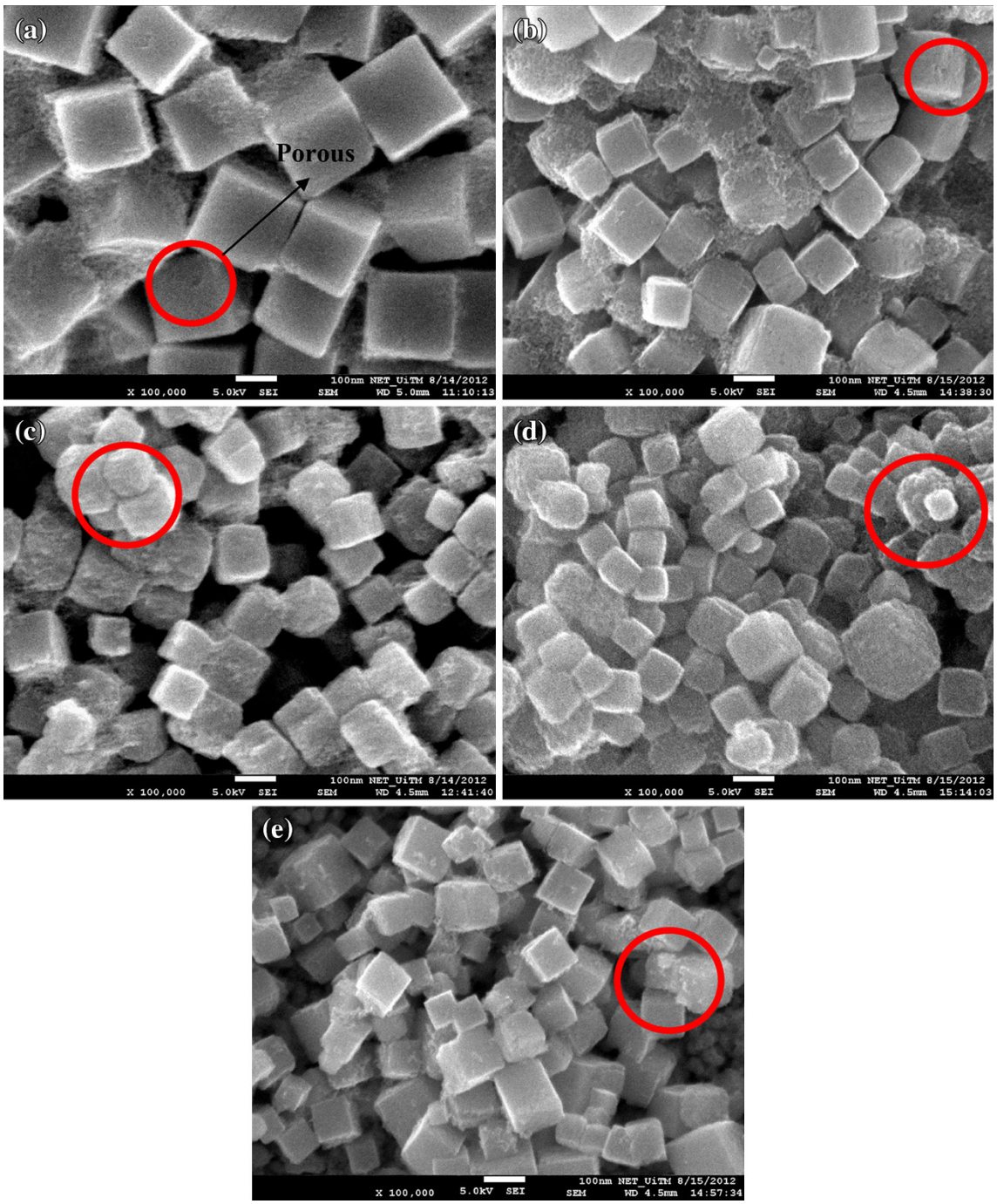

Fig. 1 FESEM morphology of nanocubic structured ZnO/SnO_2 thin films deposited at various molar ratio of Zn:Sn. **a** 1:10, **b** 3:10, **c** 5:10, **d** 7:10, **e** 10:10 and **f** 13:10

of nanocubic structured ZnO/SnO_2 from 40 to 90 RH%. The sensor performs ohmic behavior with the supplied voltage −5 to 5 V. The sensitivity was calculated using the expression (3) (Mohseni Kiasari et al. 2012).

$$S = \frac{R_a}{R_{rh}} \tag{3}$$

S is sensitivity, R_a is resistance of the sensor in air and R_{rh} is resistance in the different RH%. The values of sensitivity were presented in Fig. 8. All sensors of nanocubic structured ZnO/SnO_2 show sensitivity properties towards humidity. From the graph, the value of the sensitivity increased linearly as addition of molar Zn. Molar ratio

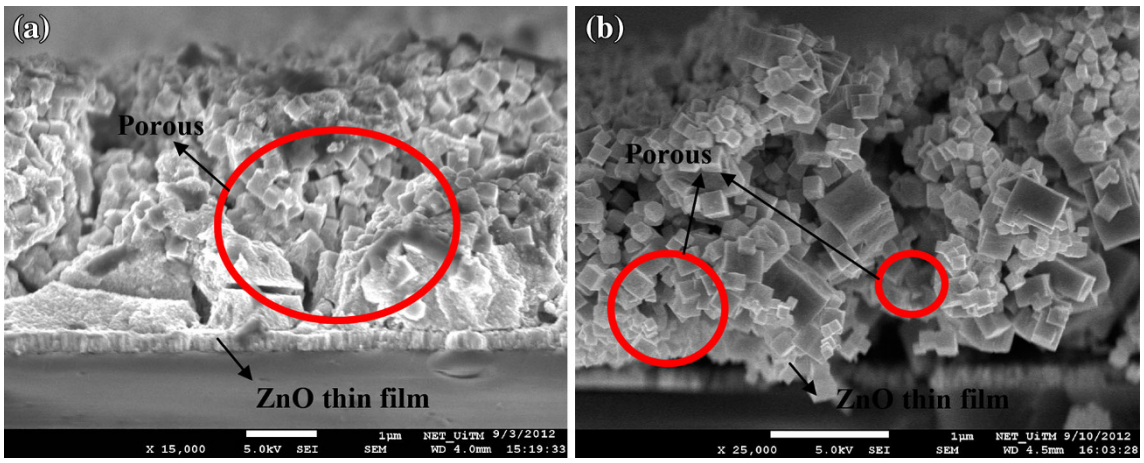

Fig. 2 FESEM images of cross-sectional view of nanocubic structured ZnO/SnO_2 thin films at molar ratio. **a** 1:10 and **b** 10:10

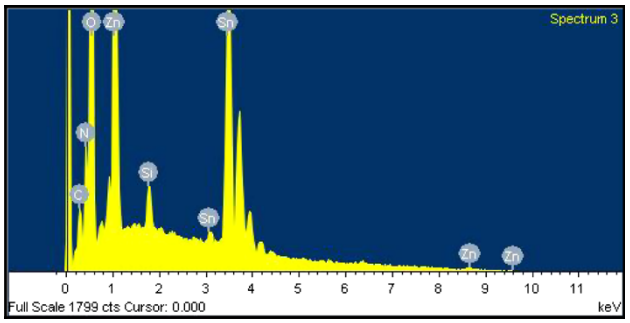

Fig. 3 EDS spectra of molar ratio 10:10 nanocubic structured ZnO/SnO_2

10:10 of nanocubic structured ZnO/SnO_2 shows the highest sensitivity value. The porosity that can be seen from the surface morphology as shown in Fig. 1 was significantly favoring the sensor humidity properties for every sensor. The sensitivity of the sensor was also dependent on the porosity (Zhang and Zhang 2008). The highest sensitivity of molar ratio 10:10 of nanocubic structured ZnO/SnO_2 was owing to the high surface reaction for adsorption and desorption process. Besides, the size of molar ratio 10:10 of nanocubic structured ZnO/SnO_2 was the smallest size structure among others sensors (Mohseni Kiasari et al. 2012). The existence of Zn–O–Sn bond thus improved the sensitivity properties. The higher Zn–O–Sn ratio favorable for Zn–O–Sn to absorb more water molecules (Yuan et al. 2010).

The resistance decreases almost linearly as a function of relative humidity as shown in Fig. 9. About two order changes in resistance of molar ratio 10:10 of nanocubic structured ZnO/SnO_2 at 40 RH% is 4.67×10^{11} and 90 RH% is 4.5×10^{9}. Further property measurements of humidity sensor characteristics such as response and

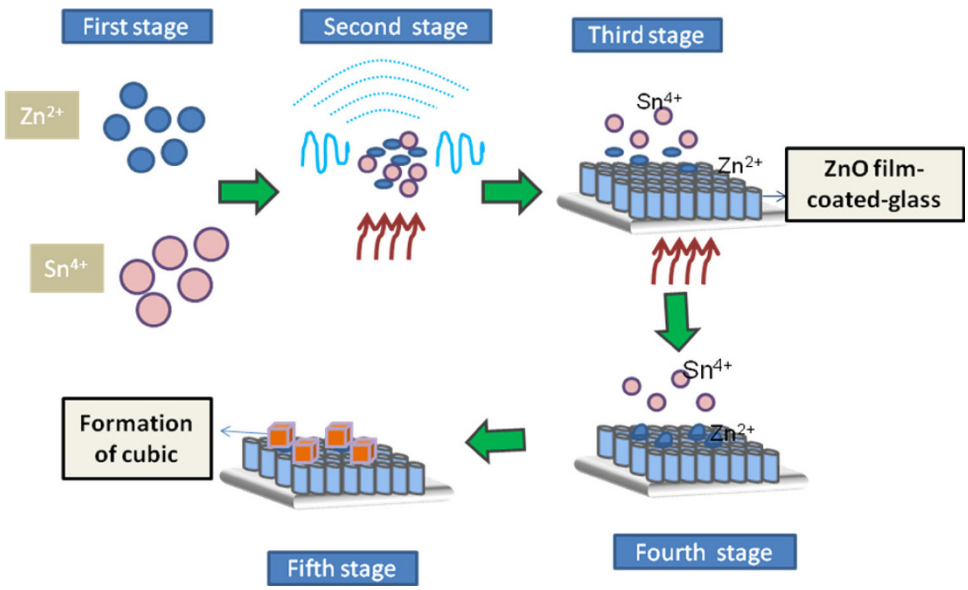

Fig. 4 Diagram of nanocubic structured ZnO/SnO_2 onto ZnO catalyst development process

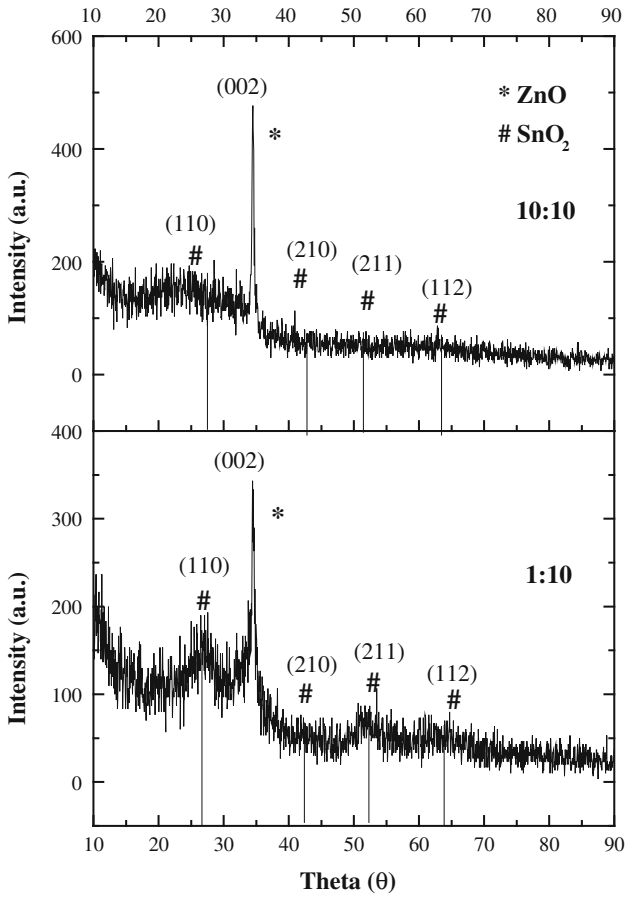

Fig. 5 XRD spectra of nanocubic structured $ZnSnO_3$ at molar ratio 1:10 and 10:10

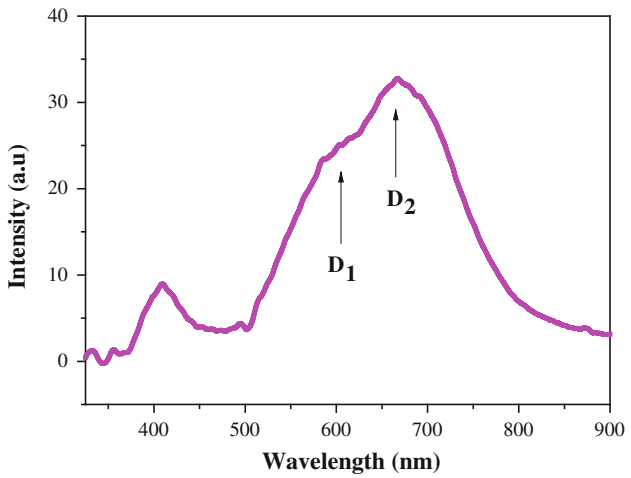

Fig. 6 Photoluminescence spectra of nanocubic structured ZnO/SnO_2 at various molar ratio

recovery time, reproducibility and stability for molar ratio 10:10 of nanocubic structured ZnO/SnO_2 were conducted.

Figure 10 shows the response and recovery curves of molar ratio 10:10 of nanocubic structured ZnO/SnO_2. From Fig. 10, the predicted value of response and recovery time constant using the following equation (4) (Mamat et al. 2011):

$$I(t) = I_0\left(1 - e\left(-\frac{t}{t_r}\right)\right) \text{ for the response time (absorption process)} \quad (4)$$

$$I(t) = I_0 e\left(-\frac{t}{t_d}\right) \text{ for the recovery time (desorption process)}$$

where I is magnitude of the current, I_0 is the saturated current, t is the time, t_r is the response time constant, t_d and is the recovery time constant. The time taken of the transition total current to become constant from 40 to 90 RH% (adsorption process) is assigned as response time and 90 to 40 RH% (desorption process) for the recovery time. The response time of the sensor is about 411 s and the recovery time is about 98 s. The repeatability performance of molar ratio 10:10 of nanocubic structured ZnO/SnO_2 were conducted by applying voltage 5 V for 4 cycles is shown in Fig. 11. The sensor has potential to reproduce slightly the same behavior although has it been exposed to the absorption and desorption process repeatedly. The stability characteristic of molar ratio 10:10 of nanocubic structured ZnO/SnO_2 tested for 5 days is shown in Fig. 12. From the result, it could be concluded that the sensor has good stability with nearly constant resistance during the measurement for 5 days at 50, 70 and 80 RH%.

The mechanism of humidity sensing of molar ratio 10:10 of nanocubic structured ZnO/SnO_2 are discussed as follows. Surface area plays an important medium for reaction between free carrier and environment. The conductivity of the sensor increases as the RH% increases due to the reaction of water molecules on the film surface. When the sensor film were surrounded by air, the surface film was covered with chemisorbed oxygen ions (O^-,O^{2-} and O_2). These oxygen ions accumulate at the film surface adsorbed by surface film of nanocubic structured ZnO/SnO_2. Generally, two forms of adsorption process occur during the surface film exposure to humidity. At low humidity the chemisorbed lead to generate with a small amount of water molecules exposed to the nanocubic structured ZnO/SnO_2. The water molecules adsorbed on the nanocubic structured ZnO/SnO_2 react reversibly with Zn lattice according to the following reaction (Chang et al. 2010):

$$H_2O + O_0 + 2Zn_{zn} \leftrightarrow 2(OH - Zn) + V^{oo} + 2e^- \quad (5)$$

where O_0 is the oxygen ion sitting on an oxygen lattice site and V^{oo} is the vacancy created at the oxygen site as following reaction (Qi et al. 2009):

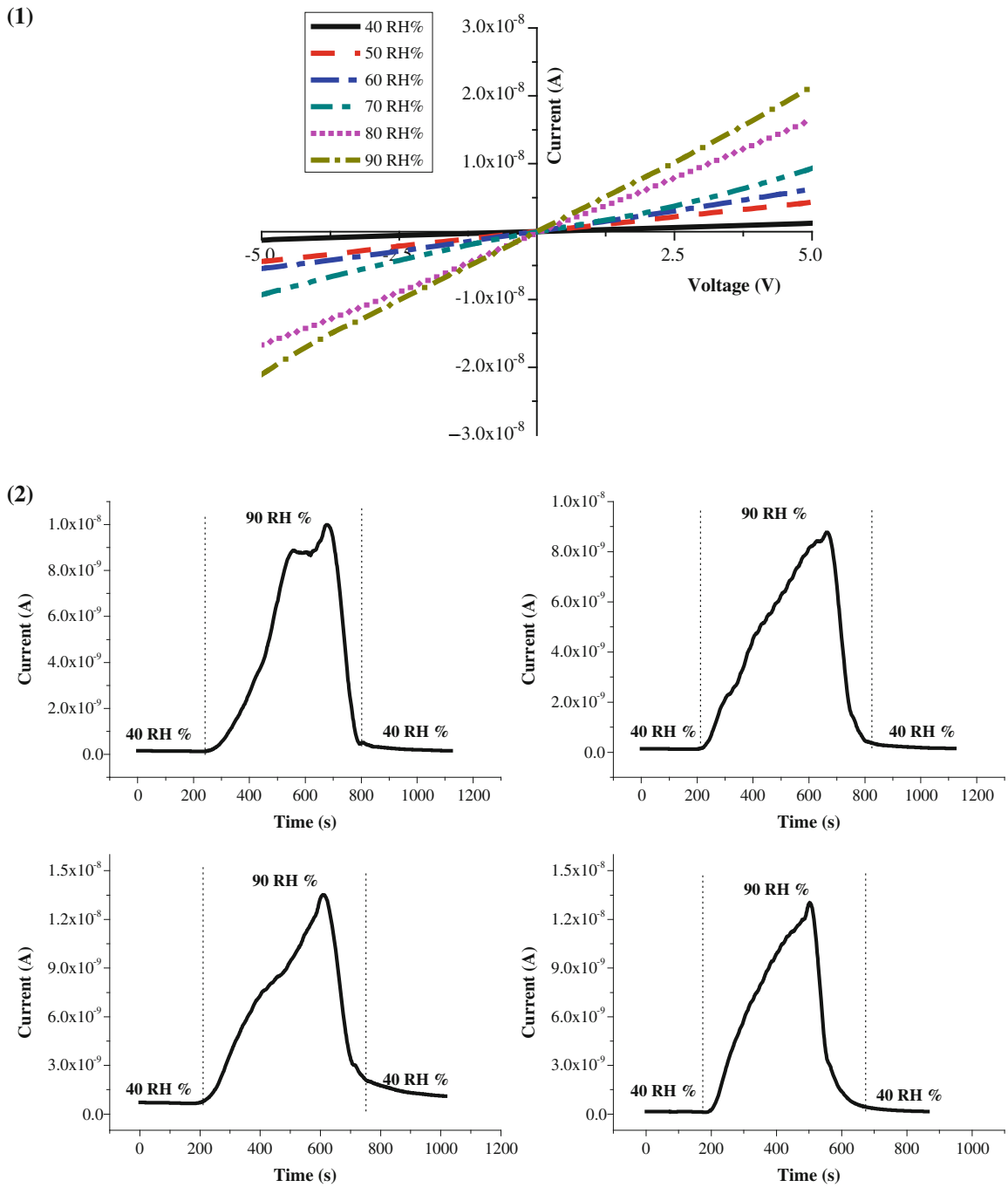

Fig. 7 *I–V* measurement of molar ratio 10:10 nanocubic structured ZnO/SnO_2 at different RH%

$$O_0 \leftrightarrow O^{2-} + V^{oo} \quad (6)$$

The dissociated OH^- and H^+ of water was adsorbed on the surface of Zn^{2+} and Sn^{4+} and associate with ionized oxygen to form the hydroxyl groups as the following reaction (Bauskar et al. 2012):

$$H^+ + O^{2-} \leftrightarrow OH^- \quad (7)$$

The free electrons accumulate at the film surface and the resistance nanocubic structured ZnO/SnO_2 film decrease with increasing RH%. The protons jump to available site that possible to conduct thus the resistance of nanocubic

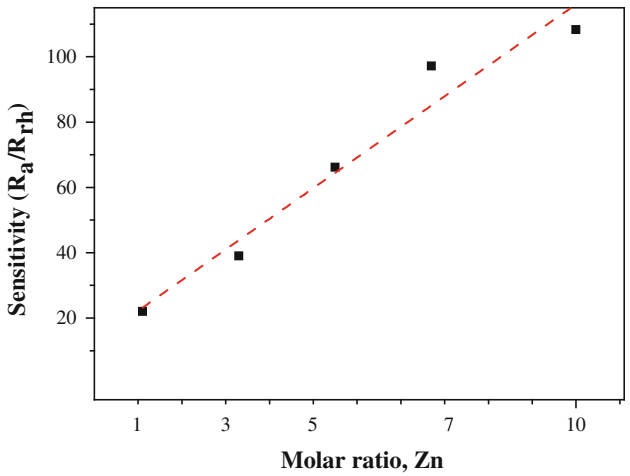

Fig. 8 Sensitivity of molar ratio 10:10 nanocubic structured ZnO/SnO_2 as function of RH%

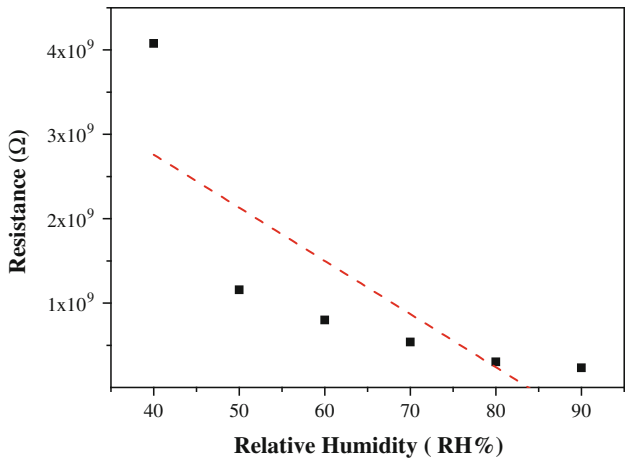

Fig. 9 The variation of resistance of molar ratio 10:10 nanocubic structured ZnO/SnO_2 as a function of RH%

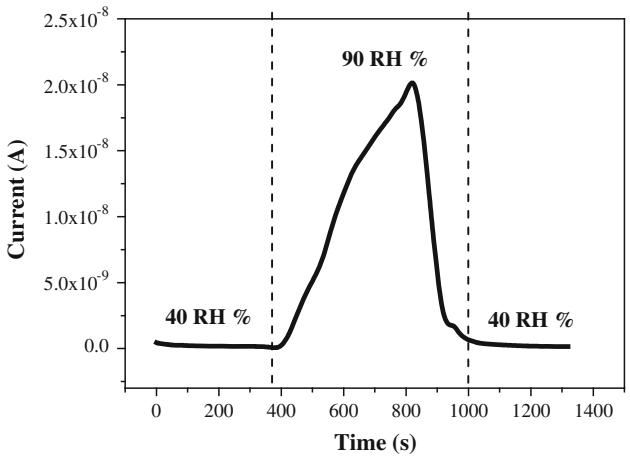

Fig. 10 Response and recovery times of molar ratio 10:10 nanocubic structured ZnO/SnO_2

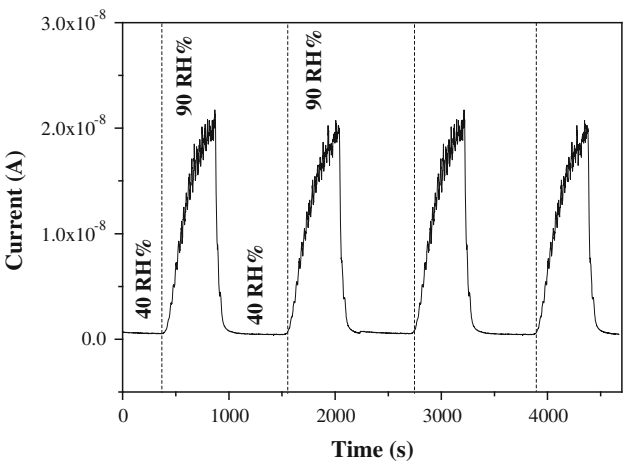

Fig. 11 Repeatability of the sensor performance of molar ratio 10:10 nanocubic structured ZnO/SnO_2

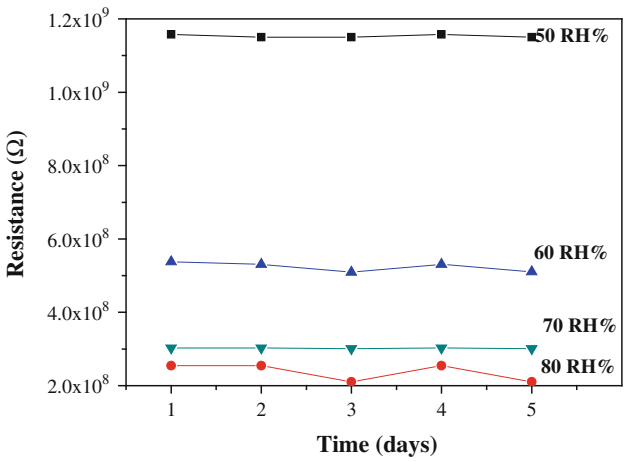

Fig. 12 The stability of the sensor for molar ratio 10:10 nanocubic structured ZnO/SnO_2 for 5 days at 50, 60, 70 and 80 RH %

structured ZnO/SnO_2 is high (Namazi and Ahmadi 2011; Faia et al. 2009).

As the humidity increases, the amount of water increases. The water molecule was reacting with the nanocubic structured ZnO/SnO_2 (physically absorbed). At this condition, H_2O is the water molecule, H^+ is the ion released, and OH^- is the water vapor that was absorbed by Zn^{2+} and Sn^{4+}. As the H^+ ions move freely together with the water, the decrease in resistance of the film due to conduction occurs (Shah and Kotnala 2012). The Grotthuss transport mechanism prompts the proton conductions to occur since proton was the dominant carrier responsible for the electrical conductivity (Chen and Lu 2005; Bauskar et al. 2012). This Grotthuss transport mechanism conducted through the proton tunnel from one water molecule to the next tunnel via hydrogen binding as illustrated in Fig. 13. The porosity of our sensor would also lead the performance of the humidity sensor properties.

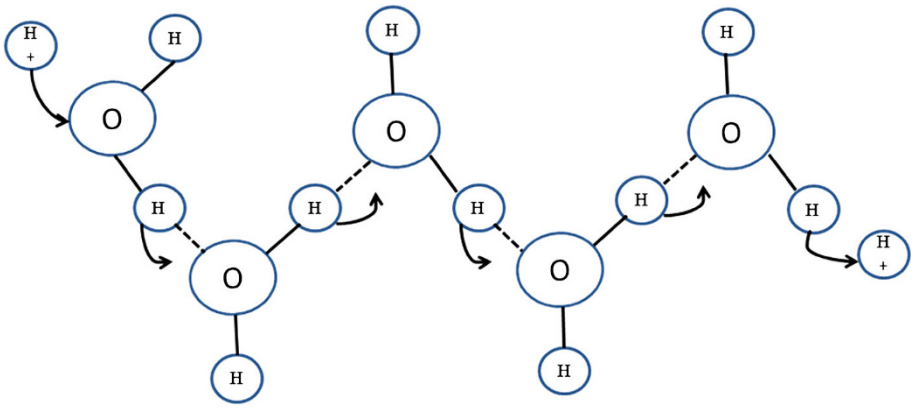

Fig. 13 The Grotthuss mechanism

Conclusion

In this work, nanocubic structured ZnO/SnO_2 was synthesized by various molar ratios via sol–gel immersion technique. From the FESEM image, the size of nanocubic structured ZnO/SnO_2 decrease as addition of molar Zn. The smallest size of nanocubic structured ZnO/SnO_2 was revealed at the surface morphology of molar ratio 10:10 with size around 50–70 nm. The PL spectra depict that nanocubic structured ZnO/SnO_2 had low intensity at UV emission region at around 400 nm and broad emission was dominant in the visible region at around 600 nm. The humidity sensing properties of nanocubic structured ZnO/SnO_2 were studied. The optimum sensitivity performed at molar ratio 10:10 of nanocubic structured ZnO/SnO_2 with ratio 104 times of $R_{40\mathrm{RH}\ \%}$ to $R_{90\mathrm{RH}\ \%}$. The sensor of molar ratio 10:10 of nanocubic structured ZnO/SnO_2 demonstrate 411 s response times and recovery 98 s times. In addition, this sensor also shows repeatability characteristic and good in stability. Hence, nanocubic structured ZnO/SnO_2 has great potential for humidity sensor application.

Acknowledgments The main author (Nor Diyana Md Sin) would like to express her thanks to Institute of Science and Faculty of Mechanical UiTM for providing the laboratory facilities. Thanks also to Ministry of Higher Education (MOHE) for financial support. The authors thank Mrs. Nurul Wahida (UiTM Asst. Science Officer), Mr Shahril and Mr Daniel (UiTM technician) for their kind support of this research.

References

Acharya R, Zhang YQ, Cao XA (2012) Characterization of zinc-tin-oxide films deposited by thermal co-evaporation. Thin Solid Films 520(19):6130–6133

Baruah S, Dutta J (2011) Zinc stannate nanostructures: hydrothermal synthesis. Sci Technol Adv Mater 12:013004

Bauskar D, Kale BB, Patil P (2012) Synthesis and humidity sensing properties of $ZnSnO_3$ cubic crystallites. Sens Actuators B Chem 161(1):396–400

Cao H, Liang RL, Qian D, Shao J, Qu M (2011) L-Serine-assisted synthesis of superparamagnetic Fe_3O_4 nanocubes for lithium ion batteries. J Phys Chem C 115(50):24688–24695

Chang SP, Chang SJ, Lu CY, Li MJ, Hsu CL, Chiou YZ, Hsueh TJ, Chen I (2010) A ZnO nanowire-based humidity sensor. Superlattices Microstruct 47(6):772–778

Chen Z, Lu C (2005) Humidity sensors: a review of materials and mechanisms. Sensor Lett 3(4):274–295

Faia PM, Ferreira AJ, Furtado CS (2009) Establishing and interpreting an electrical circuit representing a TiO_2–WO_3 series of humidity thick film sensors. Sens Actuators B Chem 140(1):128–133

Fan H, Ai S, Ju P (2010) Room temperature synthesis of zinc hydroxystannate hollow core-shell microspheres and their hydrothermal growth of hollow core-shell polyhedral microcrystals. CrystEngComm 13(1):113–117

Fan H, Zeng Y, Xu X, Lv N, Zhang T (2011) Hydrothermal synthesis of hollow $ZnSnO_3$ microspheres and sensing properties toward butane. Sens Actuators B Chem 153(1):170–175

Fouad OA, Glaspell G, El-Shall MS (2008) Growth and characterization of ZnO, SnO_2 and ZnO/SnO_2 nanostructures from the vapor phase. Top Catal 47(1):84–96

Gu L, Zheng K, Zhou Y, Li J, Mo X, Patzke GR, Chen G (2011) Humidity sensors based on ZnO/TiO_2 core/shell nanorod arrays with enhanced sensitivity. Sens Actuators B Chem 159(1):1–7

Hadia NMA, Ryabtsev SV, Domashevskaya EP, Seredin PV (2009) Structure and photoluminescence properties of SnO_2 nanowires synthesized from SnO powder. Eur Phys J Appl Phys 48(01):10603–10608

Han N, Chai L, Wang Q, Tian Y, Deng P, Chen Y (2010) Evaluating the doping effect of Fe, Ti and Sn on gas sensing property of ZnO. Sen Actuators B Chem 147(2):525–530

Hemmati S, Firooz AA, Khodadadi AA, Mortazavi Y (2011) Nanostructured SnO_2–ZnO sensors: highly sensitive and selective to ethanol. Sens Actuators B Chem 160(1):1298–1303

Hoel CA, Amores JMG, Álario-Franco MA, Gaillard JF, Poeppelmeier KR (2010) High-pressure synthesis and local structure of corundum-type In2 − 2 x Zn x Sn x O3 (x ≤ 0.7). J Am Chem Soc 132(46):16479–16487

Ji X, Huang X, Liu J, Jiang J, Li X, Ding R, Yu Y, Wu F, Li Q (2010) Hydrothermal synthesis of novel Zn_2SnO_4 octahedron microstructures assembled with hexagon nanoplates. J Alloy Compd 503(2):L21–L25

Jin C, Kim H, An S, Lee C (2012) Highly sensitive H_2S gas sensors based on CuO-coated $ZnSnO_3$ nanorods synthesized by thermal evaporation. Ceram Int 38(7):5973–5978

Li Z, Li X, Zhang X, Qian Y (2006) Hydrothermal synthesis and characterization of novel flower-like zinc-doped SnO_2 nanocrystals. J Cryst Growth 291(1):258–261

Lin C-C, Chiang Y-J (2012) Feasibility of using a rotating packed bed in preparing coupled ZnO/SnO_2 photocatalysts. J Ind Eng Chem 18(4):1233–1236

Lu L, Zhang A, Xiao Y, Gong F, Jia D, Li F (2012a) Effect of solid inorganic salts on the formation of cubic-like aggregates of $ZnSnO_3$ nanoparticles in solventless, organic-free reactions and their gas sensing behaviors. Mater Sci Eng B 177(12):942–948

Lu G, Xu J, Sun J, Yu Y, Zhang Y, Liu F (2012b) UV-enhanced room temperature NO_2 sensor using ZnO nanorods modified with SnO_2 nanoparticles. Sens Actuators B Chem 162(1):82–88

Mamat MH, Khusaimi Z, Musa MZ, Malek MF, Rusop M (2011) Fabrication of ultraviolet photoconductive sensor using a novel aluminium-doped zinc oxide nanorod–nanoflake network thin film prepared via ultrasonic-assisted sol–gel and immersion methods. Sens Actuators A 171(2):241–247

Martínez DY, Pérez RC, Delgado GT, Ángel OZ (2012) Structural, morphological, optical and photocatalytic characterization of ZnO-SnO_2 thin films prepared by the sol-gel technique. J Photochem Photobiol A Chem

Md Sin ND, Fuad Kamel M, Alip RI, Mohamad Z, Rusop M (2011) The electrical characteristics of aluminium doped zinc oxide thin film for humidity sensor applications. Adv Mater Sci Eng 2011

Mohseni Kiasari N, Soltanian S, Gholamkhass B, Servati P (2012) Room temperature ultra-sensitive resistive humidity sensor based on single zinc oxide nanowire. Sens Actuators A 182: 101–105

Namazi H, Ahmadi H (2011) Improving the proton conductivity and water uptake of polybenzimidazole-based proton exchange nanocomposite membranes with TiO_2 and SiO_2 nanoparticles chemically modified surfaces. J Power Sources 196(5): 2573–2583

Qi Q, Zhang T, Zeng Y, Yang H (2009) Humidity sensing properties of KCl-doped Cu–Zn/CuO–ZnO nanoparticles. Sens Actuators B Chem 137(1):21–26

Rittersma ZM (2002) Recent achievements in miniaturised humidity sensors—a review of transduction techniques. Sens Actuators A 96(2):196–210

Shah J, Kotnala RK (2012) Humidity sensing exclusively by physisorption of water vapors on magnesium ferrite. Sens Actuators B Chem 171–172:832–837

Song X, Qi Q, Zhang T, Wang C (2009) A humidity sensor based on KCl-doped SnO_2 nanofibers. Sens Actuators B Chem 138(1): 368–373

Su Y, Zhu L, Xu L, Chen Y, Xiao H, Zhou Q, Feng Y (2007) Self-catalytic formation and characterization of Zn_2SnO_4 nanowires. Mater Lett 61(2):351–354

Sun P, Sun Y, Ma J, You L, Lu G, Fu W, Li M, Yang H (2011) Synthesis of novel SnO_2/$ZnSnO_3$ core–shell microspheres and their gas sensing properties. Sens Actuators B Chem

Sun P, You L, Sun Y, Chen N, Li X, Sun H, Ma J, Lu G (2012) Novel Zn-doped SnO_2 hierarchical architectures: synthesis, characterization, and gas sensing properties. CrystEngComm 14(5): 1701–1708

Sundaram R (2007) Comparative study on micromorphology and humidity sensitive properties of thick film and disc humidity sensors based on semiconducting $SnWO_4$-SnO_2 composites. Sens Actuators B Chem 124(2):429–436

Tang Y, Jiang Y, Jia Z, Li B, Luo L, Xu L (2006) Synthesis of $CdSnO_3 \cdot 3H_2O$ nanocubes via ion exchange and their thermal decompositions to cadmium stannate. Inorg Chem 45(26): 10774–10779

Wang X, Zhang J, Zhu Z, Zhu J (2007a) Humidity sensing properties of Pd^{2+}-doped ZnO nanotetrapods. Appl Surf Sci 253(6): 3168–3173

Wang WW, Zhu YJ, Yang LX (2007b) ZnO–SnO_2 hollow spheres and hierarchical nanosheets: hydrothermal preparation, formation mechanism, and photocatalytic properties. Adv Funct Mater 17(1):59–64

Wang Z, Liu J, Wang F, Chen S, Luo H, Yu X (2010) Size-controlled synthesis of $ZnSnO_3$ cubic crystallites at low temperatures and their HCHO-sensing properties. J Phys Chem C 114(32): 13577–13582

Wrobel G, Piech M, Dardona S, Ding Y, Gao PX (2009) Seedless synthesis and thermal decomposition of single crystalline zinc hydroxystannate cubes. Cryst Growth Des 9(10):4456–4460

Yadav BC, Verma N, Singh S (2012) Nanocrystalline SnO_2–TiO_2 thin film deposited on base of equilateral prism as an opto-electronic humidity sensor. Opt Laser Technol 44(6):1681–1688

Yan W, Fang M, Tan X, Liu M, Liu P, Hu X, Zhang L (2010) Template-free fabrication of SnO_2 hollow spheres with photoluminescence from Sni. Mater Lett 64(19):2033–2035

Yuan Q, Li N, Tu J, Li X, Wang R, Zhang T, Shao C (2010) Preparation and humidity sensitive property of mesoporous ZnO–SiO_2 composite. Sens Actuators B Chem 149(2):413–419

Zeng J, Wang H, Zhang YC, Zhu MK, Yan H (2007) Hydrothermal synthesis and photocatalytic properties of pyrochlore $La_2Sn_2O_7$ nanocubes. J Phys Chem C 111(32):11879–11887

Zhang WH, Zhang WD (2008) Fabrication of SnO_2/ZnO nanocomposite sensor for selective sensing of trimethylamine and the freshness of fishes. Sens Actuators B Chem 134(2):403–408